Plasmonic nanocomposites based on silver nanocube-polymer blends displaying Nearly Perfect Absorption in the UV region

Florent Pourcin, Clément A Reynaud, Miriam Carlberg, Judikaël Le Rouzo, David Duche, Jean-Jacques Simon, Ludovic Escoubas, Rose-Marie Sauvage, Gerard Berginc, Olivier Margeat, et al.

Plasmonic nanocomposites based on silver nanocube-polymer blends displaying Nearly Perfect Absorption in the UV region

Florent Pourcin, [1] *Clément A. Reynaud,* [2] *Miriam Carlberg,* [2] *Judikaël Le Rouzo,* [2] *David Duché,* [2] *Jean-Jacques Simon,* [2] *Ludovic Escoubas,* [2] *Rose-Marie Sauvage,* [3] *Gérard Berginc,* [4] *Olivier Margeat*[1]* *and Jörg Ackermann.* [1]*

1. Aix-Marseille Univ, CNRS, CINaM UMR 7325, 13288 Marseille, France.

2. Aix Marseille Univ, CNRS, Université de Toulon, IM2NP UMR 7334, 13397, Marseille, France.

3. DGA/DS/MRIS, 75015 Paris, France.

4. Thales Optronics, 78990, Elancourt, France.

[*] Corresponding Authors:

E-mail address: olivier.margeat@univ-amu.fr ; jorg.ackermann@univ-amu.fr

KEYWORDS

nanocomposites, plasmonic, silver nanocubes, thin films, perfect absorber

ABSTRACT

Plasmonic nanocomposites based on well-dispersed silver nanocubes in poly(vinyl-pyrrolidon) are presented that are solution-processed into layer of varying volume fraction of nanocubes. We show that the high-energy modes of the nanocubes are almost insensitive to plasmonic coupling within the nanocubes assemblies, leading to linear increase of light absorption in the UV with the nanocube densities. Concerning the main dipolar resonance mode at 450 nm, it is strongly affected by the formation of these assemblies, leading to an increased absorption in the UV as well as large absorption band in the visible. Simulations of the optical response of the nanocube assemblies as a function of nanocube spacing and electric field polarization reveal that optical features in the visible are due to inter-cube couplings at short inter-cube distances and parallel electric field orientation. In contrast, the additional plasmonic band in the UV has its origin in residual dipolar oscillations of the nanocubes in combination with weak dipolar coupling for both parallel and transversal field polarization. The combination of these effects leads to an enlarged absorption band in the UV with nearly perfect light absorption of 98.8% at high silver volume fraction of 8% that is accompanied by a very weak specular reflection of only 0.28 %. While such perfect absorption is usually only observed when nanocubes are assembled on gold surface, nearly perfect absorption herein is achieved on a large palette of substrates including glass, plastic and cheap metals such as aluminum, making it a promising approach for solution-processed robust and cheap quasi perfect absorption coatings.

Introduction

Plasmonic nanocomposite materials based on metal nanoparticles embedded in a polymer-based dielectric are an emerging class of optical materials.[1,2] They combine the

tunability in plasmonic resonance of metal nanoparticles with simplicity in processing and mechanical properties of polymers. Over the last years, such plasmonic polymer nanocomposite (p-PNC) approaches have led to novel optical materials with tunable optical properties that can be integrated into manifold of applications such as optical sensors and optoelectronic device structures.[3] In general, there are two approaches to produce p-PNC, which are either based on in situ synthesis of metal nanoparticles in the polymer or separate synthesis of nanoparticles by colloidal chemistry followed by blending the nanoparticles with the polymer into a p-PNC. The latter one allows synthesizing monodispersed nanoparticles with different shapes independently of the choice of polymer. This makes this approach a more versatile for the synthesis of p-PNC with novel optical properties. Indeed the use of shaped nanoparticles such as nanorods, nanocubes or nanoprisms is of particular interest as they can generate high electromagnetic field enhancement at corners and edges compared to nanospheres, as well as higher order localized surface plasmon resonances (SPRs).[4–7] For example, it has been shown that the plasmonic absorption of gold nanorods embedded in a polymer can be tuned by increasing the volume fraction of the nanoparticle inside the p-PNC.[4] The plasmon resonance peak of the gold nanorods exhibits a red shift with increasing volume fraction and coupling is observed for interparticle distances up to 70 nm.

Amongst shaped metal nanoparticles, silver nanocubes (NCs) are outstanding plasmonic nanoparticles as they show not only intense plasmonic coupling leading to strong enlargement of the plasmonic absorption.[5–8] Assembly of monolayers on dielectric substrates generates broadband absorption of strong light polarization dependence,[8,9] while their assembly on metal surface leads to highly tunable optical properties and most importantly to efficient and zero reflection coating.[5,10,11] All these approaches use generally monolayer of NCs and thus 2D

assembly of such objects. Here, we use a simple p-PNC approach to assemble nanocubes at varying concentration in a 3D fashion inside a polymer film. The variation of the NCs concentration allows us controlling the coupling amongst the nanoparticles inside p-PNC layers and thus their optical response on various substrates. Recently, we have developed such p-PNC based on randomly dispersed silver nanospheres and NCs blended in a dielectric polymer host matrix. The optical properties as a function of nanoparticle shape were studied to determine the complex optical indices of the nanocomposites by spectroscopic ellipsometry.[12] As the volume fraction of the nanoparticles inside the polymer matrix was very low, the optical properties of the p-PNCs were governed by individual nanoparticles without observation of plasmonic coupling between NCs. In order to introduce coupling between the NCs inside the p-PNC, higher volume fraction inside the polymer matrix are needed. However, the increase of nanoparticle density inside the blend leads generally to the formation of aggregates due to immiscibility issues and depletion attraction.[13] Such aggregates would rather increase reflection due to light scattering than increase light absorption. Additionally, in the presence of interfaces, nanoparticles can migrate to interfaces producing anisotropic films with accumulation of nanoparticles near the substrate[14] due to entropic-push transition induced by the surfaces.[13] In order to produce highly-loaded aggregate-free p-PNCs, it is necessary to control the interaction between the polymer host and the ligands of the metal nanoparticles to improve their miscibility within the polymer. [4,15]

We report here p-PNCs based on homogeneously dispersed silver NCs embedded in poly(vinyl-pyrrolidon) (PVP) with volume fraction of NCs up to 8%. The high dispersion of the NCs and thus the suppression of aggregate formation during layer processing was obtained by using highly monodisperse NCs covered with PVP. The p-PNCs films processed on glass substrates shows optical properties that are dominated by the high energy modes of the NCs in

the UV. Indeed, these modes are only weakly affected by plasmonic coupling and increase almost linearly with the concentration of the NCs. When coupling between NCs starts to get dominant inside the films by the formation of NC assemblies, we observe two phenomena. First, inter-cube coupling mode appears in the visible range that leads to red-shifted absorption bands when reducing inter-cube distance.[8,16–19] This limits the possibility to reach strong light absorption in the spectral region of the dipolar resonance. Secondly, the light absorption in the UV is enhanced by a blue-shift of the dipolar mode. Polarization dependent simulations reveal that the parallel electric field orientation, i.e. in the plane of the assemblies, generates plasmonic excitation leading to the red-shifted inter-cube coupling mode, as well as the blue-shifted dipolar mode. Furthermore, a transverse electric field orientation, i.e. out of the plane of the assemblies, leads only to the blue-shifted dipolar plasmonic excitations. Thus, the inherence of the high-energy modes together with the blue-shift of the dipolar mode towards the UV region at high volume fraction of NCs generate an enlarged band in the UV with nearly perfect light absorption of 98.8%. We investigate herein the compatibility of theses p-PNC with industrial relevant substrates such metals and plastic to produce such nearly perfect absorption.

Experimental part

Materials:

Ethylene glycol (EG, 99%), silver trifluoroacetate (99,99%), Poly(vinyl pyrrolidon) (PVP , Mw 55000), Poly(methyl methacrylate) (PMMA, Mw 120000), Sodium hydrosulfide hydrate, Ethanol anhydrous and aqueous hydrochloric solution (HCl, 37%) were purchased from Aldrich.

Synthesis of Silver NCs:

The silver NCs were synthesized according to a previously published polyol process by Zhang et al.[20] but with slight modifications. In a typical synthesis, 20 mL of EG were added into a 100 mL flask and heated 25 min under stirring in an oil bath at 170°C. Then 0,250 mL of NaSH (3mM in EG) were injected to the solution. Two minutes later, 2 mL of HCl (3 mM in EG) and 5 mL of PVP (20mg/mL in EG) were respectively added to the mixture. As a last step, 1.6 mL of silver trifluoroacetate (282 mM in EG) were injected into the solution after two minutes. Importantly, the flask was kept capped with a glass stopper for the entire process except during the introduction of reagents. The reaction was stopped by placing the flask in an ice-water bath after 30 min of heating to obtain the desirable size. The formed nanoparticles were washed by ethanol and deionized water twice then dispersed in 5 mL deionized water.

Solution and thin films preparation:

A determinate volume of the initial nanoparticles solution was centrifuged and washed twice with anhydrous ethanol to eliminate any remaining traces of water. Then the precipitate was dispersed in PVP (40 mg/mL in anhydrous ethanol) and put in a sonicated bath to obtain complete dispersion. The spin-coating speed (1500 rpm) as well as PVP concentration were optimized to obtain high-quality thin films prepared in argon-filled glovebox on glass substrates. Different concentrations of NCs were used to study the optical effects of NCs density within the layer. The film thickness was measured by a contact profilometer Dektak XTS (Bruker, Germany) equipped with a stylus of 2µm radius.

Electron Microscopy:

Transmission electron microscopy (TEM) analysis was performed using a JEOL JEM-3010 operating at 300kV. For the samples preparation, a modification of the polymer floating layer technique was applied.[21] In details, PVP layers containing the nanoparticles were spin-coated on a PMMA layer (pre-deposited on glass substrate: 1500 rpm at 20 mg/mL in toluene). The substrate was then immersed in toluene to easily dissolve the PMMA, allowing to peel off a piece of the PVP layer and deposit it on the TEM holey grid. The surface coverage was determined from the TEM images using the ImageJ particle size analysis function. A color threshold filter was employed to produce a binary image used for surface coverage calculations. Cross section images were carried out on SEM (secondary electron microscopy) with operation voltage of 15kV. AFM images were obtained by using NTEGRA Prima (NT-MDT) in tapping mode.

Optical measurements:

UV-visible optical measurements were recorded using a Perkin Elmer Lambda 950 spectrophotometer including an integrating sphere (schemes of the setup shown in **Figure S1**). The sample is placed either in front of the integrating sphere to measure the transmittance (T), or in back at an angle of 8° to measure the total reflectance (R). For diffuse reflectance measurement, the sample is kept in the same position as for total reflectance, but a port is removed to subtract the specular reflected light. Finally, the absorptance (A) is calculated by using A= 1 - T - R. The 2D mapping was measured with a Light Tec spectropolarimetric goniometer in specular reflection mode.

FDTD simulations:

Finite Difference Time Domain (FDTD) simulations were performed using the commercial software Lumerical. The simulated NCs were designed according to the information taken from the TEM images: edge length of 36 nm and a corner radius of 6 nm. The optical indices of silver were taken from J.Rumble's data,[22] the refractive index of the PVP was considered constant at 1.55 on the range of interest. The absorption and scattering cross sections of single NCs were calculated by integrating the Poynting vector of the total and scattered fields.

Results and Discussion

Optimisation of silver NCs synthesis and embedding in PVP thin films

NCs with size in the range of 30 to 40 nm are selected herein for the synthesis of p-PNCs as they show the maximum plasmonic response.[12] In general, gold and silver colloidal metal nanocrystals of controlled sizes and shapes are ideal building blocks for p-PNCs as they can be synthesized using either surfactants or polymers to selectively stabilize low-energy crystal facets and to form single-crystalline particles.[23,24] The shaped nanocrystals possess SPRs that can be easily tuned through chemical synthesis.[25] Noble metal NCs have attracted much interest in photonic applications, as they exhibit edges and corners where high local fields can arise, resulting in exceptional optical properties.[26–29] Several methods based on the polyol method have been proposed to control the synthesis of NCs with high yields.[30,31] As evidenced by theoretical and experimental results, the shape parameters such as edge length and curvature of edges and corners[32,33] as well as aggregate properties[34,35] have a great influence on the plasmonic properties of silver NCs. Therefore, silver NCs have high potential to introduce novel optical properties in p-PNCs when their density inside the nanocomposite allows couplings.

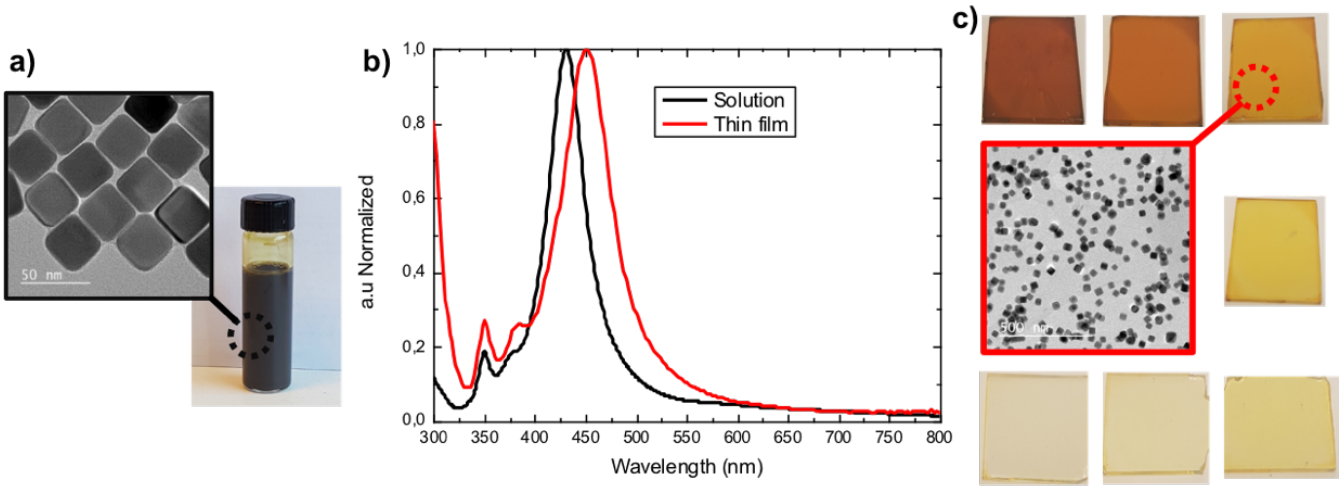

Figure 1. (a) TEM picture of silver NCs as prepared; (b) absorption spectra of silver NCs in solution (black line) and dispersed in PVP layer on glass (red line); (c) optical photographs of the composite thin films by spin-coating on glass substrates.

The NCs were synthesized following the procedure from Zhang et al. with slight modifications.[20] Briefly, the synthesis relies on a sulfide-mediated polyol method using polyvinyl-pyrrolidone (PVP) as a capping agent and shape controller. Different sizes of NCs can be obtained by adjusting the reaction time. In this study, we focus on NCs with narrow size dispersion and regular shape. An optimized NC synthesis with edge length of 36 nm and narrow size dispersion (relative standard deviation rsd= 4.1%) is shown in **Figure 1a**. The absorption spectrum of the optimized NCs in solution is shown in **Figure 1b.** We observe the three characteristic absorption bands of silver NCs at 430 nm (dipolar resonance), the shoulder at 380 nm (quadrupolar resonance)[36,37] and the peak at 350 nm (due to the sharp corners of the cubes),[12] as expected for 36 nm PVP-coated silver NCs in aqueous solution. It is worth to mention that most of the studies found in the literature attribute the main absorption of silver nanocubes to dipolar resonance,[18,36–38] however the situation is more complex with the two modes at higher energy as the origin of these modes is still discussed. Indeed, concerning the peak at 350 nm, the origin is claimed either as a silver bulk plasmon,[39,40] a quadrupolar (or multipolar) mode,[16,41,42] or

due to the rounding of the cube (corner sharpness).[12,18] Concerning the peak at 380 nm, the origin is mostly attributed to a quadrupolar mode[18,38] or quadrupolar-dipolar hybrid mode.[36]

In order to produce p-PNCs with highly dispersed NCs, PVP was used as polymer host, as it is already present as surfactant in the NCs synthesis, guarantying improved miscibility of the NCs with the PVP polymer in solution.[12,43] In order to characterize the absorption properties of the nanocomposite film by simple transmittance measurements, we selected glass as substrate while advanced optical properties were studied on a large choice of substrates including metals as shown in last sections.

We studied at first p-PNCs spin-coated on glass with low concentration of NCs. **Figure 1b** shows the UV-vis absorption spectrum of p-PNC layer using the optimized NCs. The same resonance mode absorption of the NCs is found compared to NCs in solution, i.e. the dipolar mode at 450 nm, the quadrupolar mode at 386 nm and the peak due to sharp corners at 350 nm, as expected for 36 nm silver NCs in a PVP environment on glass.[12] There is only a weak red shift of 20 nm in the dipolar resonance attributed to the change in dielectric constant of the solvent in solution to the PVP matrix in the layer. Importantly, we found that only those monodispersed NCs with nearly perfect cubic shape lead to thin films with homogeneous morphology, i.e. well-dispersed NCs within the PVP layer (yellowish film as shown in **Figure 1c** and **Figure 2**). The use of NCs with large size distribution (rsd > 5%) or shape distortion (nanorods like) gave rise to formation of silver aggregates during layer processing. This leads to additional light absorption as indicated by the shoulder at higher wavelength on the dipolar resonance peak. Additionally, the size of the NCs is also found to be critical for obtaining perfectly dispersed NCs. The NCs with edges larger than 50 nm systematically produced thin films with NCs aggregates (**Figure S2**). In the following, we selected monodispersed well-defined silver NCs with a 36 nm edge

length to process p-PNCs films with increasing NCs volume fraction in order to investigate the effect of NCs density on the optical properties of the p-PNCs.

Effect of the NCs density on the optical responses

Various concentrations of the optimized NCs were blended with PVP solutions at a constant concentration (40 mg/mL). This technique allows producing thin films with nearly same thickness over a large range of NCs density (see **Table 1**).

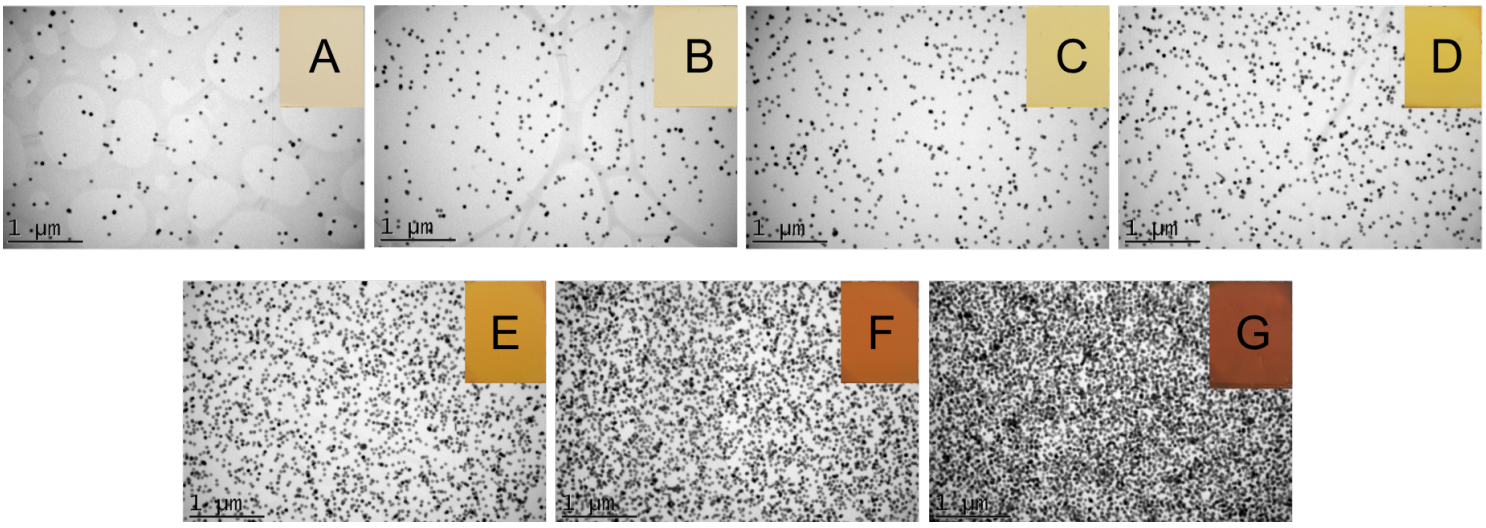

Figure 2. TEM images of the PVP thin films with different NCs densities (floating-layer technique was applied to the spin-coated thin films to deposit them on TEM holey grids).

The NCs dispersion and density in the PVP matrix as a function of silver NCs density were studied by TEM analyses of the nanocomposite layer using a modification of the floating layer technique that allow to transfer the p-PNC layers onto a carbon grid without damaging the films.[21] **Figure 2** shows the corresponding TEM images of the p-PNC films with different NC concentration (increasing from A to G). A well-dispersed organization of the NCs inside the PVP matrix without formation of NC aggregates is observed for all selected NCs

concentration, i.e. no direct contact between the cubes. The NCs are not isotropically dispersed inside the PVP but form rather ensemble of a few NCs, and only a few isolated cubes are present inside the p-PNC. This is known to occur when steric stabilization by the ligands is insufficient to balance the depletion attraction.[44] As a consequence, an increase of the volume fraction of the NCs induces mainly an increasing number of such ensemble. As it can be seen in **Figure 2**, the increase in NC density from D to G, leads to p-PNCs in which a reduction in the average distance inside the ensembles occurs as shown in **Figure S3**. Once the limit of miscibility of the NCs inside the PVP of around 8% in volume fraction is reached, small aggregates of NCs are generated during layer processing, as shown in **Figure 2** for sample F and G.

The TEM analysis were further applied to study the distribution of the NCs inside the PVP layer. By taking into account that TEM images only show 2D projection of the 310 nm thick nanocomposite layer, there is thus a limitation for deeper analyses of the cube distributions in the p-PNCs, especially for the estimation of the spacing between NCs. But the combination of TEM, SEM cross-section analyses with AFM analyses shown in **Figures 2**, **S3**, **S4** and **S5** allowed us to extract these parameters in an appropriate way.

Samples	*Number of nanocubes/µm² (rsd)*	*Volume fraction of nanocubes (%)*	*Surface coverage of nanocubes (%)*	*Thickness (nm)*
A	*11 (16%)*	0.2	2.1	*314*
B	*23 (16%)*	0.3	3.7	*313*
C	*32 (17%)*	0.5	6.0	*314*
D	*58 (15%)*	0.9	9.6	*312*
E	*167 (10%)*	2.4	25.2	*318*
F	*289 (15%)*	4.1	45.0	*328*
G	*519 (16%)*	7.7	72.6	*315*

Table 1. Summary of samples and their related morphological properties.

The density of NCs within the film was calculated using the TEM images. As it can be seen in **Table 1**, the average density of NCs per μm^2 increases from 11 cubes/μm^2 (film A) to 519 cubes/μm^2 (film G) with increased NCs concentration inside the blend solution. The density of NCs inside the blend was converted to volume fraction of NCs in the Ag-PVP composite from 0.2 to 7.7 %. Cross-section analyses were realized by SEM to visualize the vertical distribution of the NCs inside the PVP matrix. As shown in **Figure S4**, the distribution of the NCs inside the PVP is anisotropic in the case of low-density samples. A large amount of the cubes is indeed located within the first 200 nm, in contact with the glass substrate. In contrast, distribution of the NCs in sample G with the highest density presents a homogeneous distribution of cubes over the whole 315 nm of the layer. The surface region of the p-PNC layers is found mainly free of NCs, as only few cubes are observed in this region in the case of the sample G. We applied then AFM analyses to study the surface quality of the nanocomposite films as a function of NC density. **Figures S5** shows the corresponding AFM images obtained in non-contact tapping mode. Very smooth surfaces with RMS roughness as low as 0.3 nm for sample A and only 1.1 nm even in the case of the highly dense sample G are produced. This clearly indicates a high optical quality of these layers even at high NC density, lacking additional scattering effects at the layer surface. The high optical quality can be directly related to the improved solubility of the NCs in the blend solution.

In order to study the optical properties of the p-PNC as a function of NCs density, layers were deposited by spin coating on glass substrate. A complete set of optical analyses including transmission spectra and total reflectance as well as diffuse reflectance using an integrating sphere was recorded. **Figure 3a** shows the resulting absorption spectra of samples A-G, while **Figure S6** presents transmission spectra. For low NC concentration, the transmission and

absorption spectra are dominated by the plasmonic dipolar mode at 450 nm. With increasing NCs concentration, we observe several strong changes in the UV and visible regions. The main dipolar resonance mode at 450 nm is strongly affected by the increase in NCs density. Plasmonic inter-cube couplings (also referred as gap plasmon) appear within NCs assemblies and trigger an enlargement and red-shift of the absorption, with the appearance of a new large peak at 500 nm.[8,16–19] Furthermore, the absorption spectra in **Figure 3a** reveal a blue-shift of the dipolar mode at 420 nm (sample F), which is further shifted towards 405 nm for the highest concentration of NCs (sample G, marked with red triangle), enhancing the absorption in the UV.

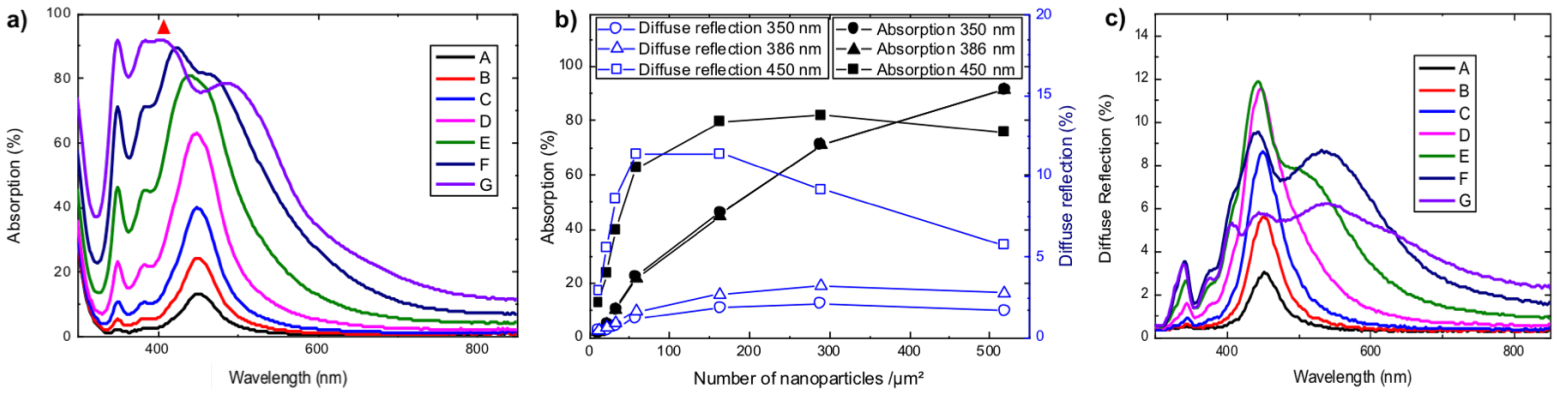

Figure 3. Absorption spectra for nanocubes-embedded PVP films A to G (a). Plot of the absorption and diffuse reflectance values at 350, 386 and 450 nm as a function of the nanocube density (b). Corresponding diffuse reflectance spectra (c).

In contrast, the quadrupolar mode at 386 nm and cubic shape mode at 350 nm are less affected by the increase of NC density. Their absorptions in the UV region increase almost linearly with increasing NCs density and become the dominant absorption modes at high NCs concentration in the p-PNC, showing for sample G absorptions of 91.5% and 91.4 % for the quadrupolar mode and cubic shape mode, respectively. The relation between NCs density and absorption of the p-PNC is presented in **Figure 3b**. It can be clearly seen that the absorptions of both high-energy modes follow almost linearly the concentration of the NCs up to the highest

concentration. In contrast, the absorption of the dipolar mode at 450 nm increases only in a linear way up to sample C and derives strongly into saturation for sample E-G, due to its slight blue-shift, reaching a maximum of 80% in absorption even for the highest NCs concentration.

In order to better understand the optical properties of the p-PNC, the diffuse reflectance can give more insights on the plasmonic coupling between NCs. As the films possess low roughness values and thus negligible surface scattering effects, we consider the diffuse reflectance to be related only to the embedded nano-objects and not to the surface. As shown in **Figure 3c**, the diffuse reflectance of samples A to C are only composed of the resonance responses of isolated NCs at 450 nm, evidencing that mainly non-interacting NCs are included in the layers.[45,46] As the density of NCs is increased in the p-PNC, diffuse reflectance show a broadening of the resonance signal at 450 nm towards higher wavelengths as it is seen for sample D. This phenomenon is even enhanced in the spectra of films E to G, as the increasing plasmonic couplings between the NCs introduce broad responses up to 800 nm. Furthermore, we observe a shoulder around 420 nm in the diffusion spectra of sample E-F that appears as a clear peak at 405 nm for the highest NCs concentration in sample G. The position of this peak corresponds to the blue-shifted dipolar resonance in the absorption spectra, suggesting that its origin and slight blue-shift are related to weak plasmonic coupling between the NCs inside the blend.

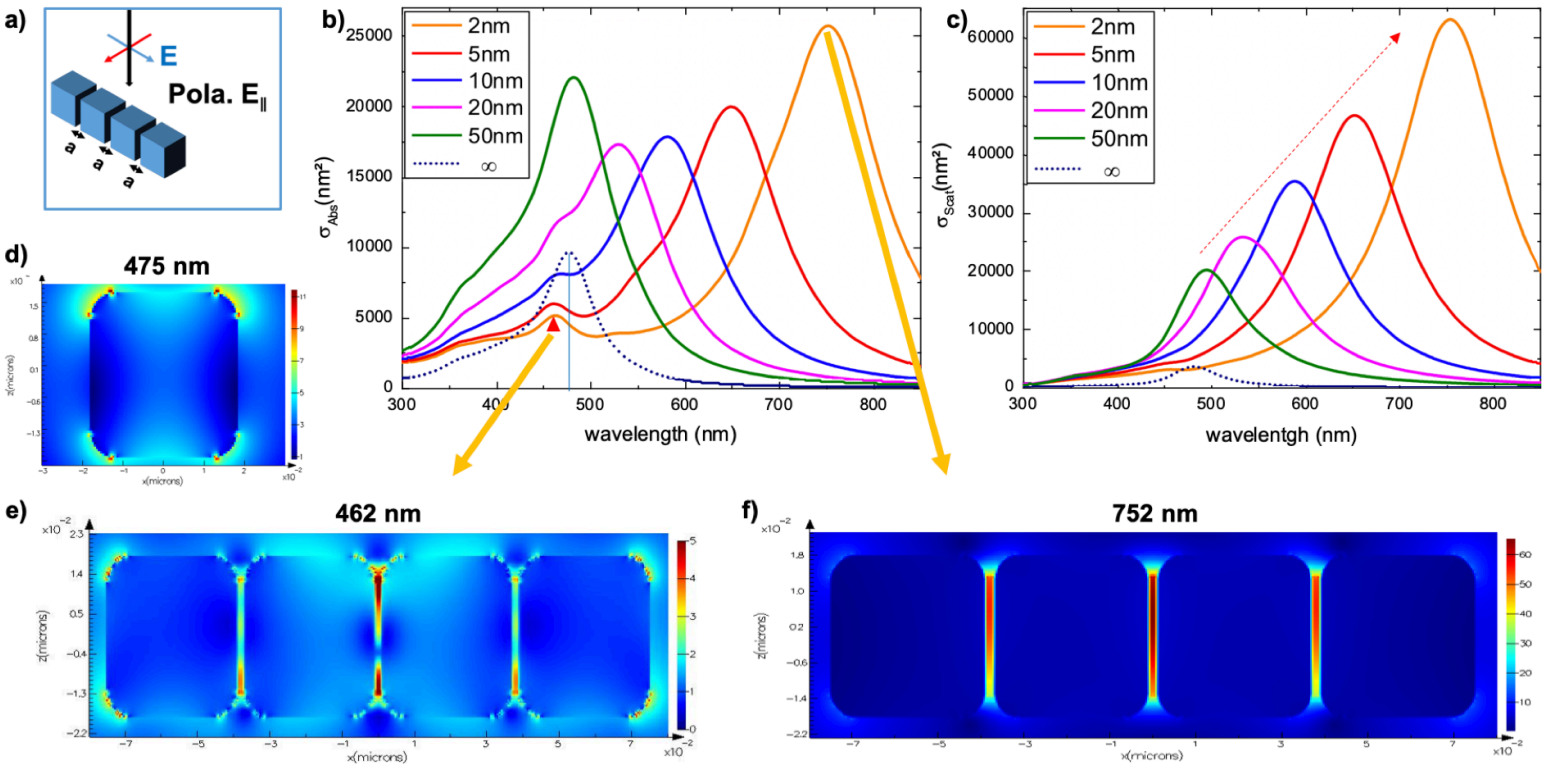

Figure 4. Simulated configuration CA showing the $E_{//}$ light polarization (a). Resulting calculated absorption cross sections (b) and scattering cross sections (c) as a function of the NCs spacing length *a*. Mapping of the electric field for a single NC at 475 nm (d) and for the four NCs with *a* = 2nm at 462 nm (e) and 752 nm (f).

In order to study these optical changes of the p-PNC more in details, especially the reinforcement of the absorption towards the UV region, we performed FDTD optical simulations of plasmonic excitation. Two types of NCs configurations were studied that correspond to typical NCs assemblies observed in the nanocomposite as shown in **Figure S3**. The first configuration CA presented in **Figure 4a** is a parallel alignment of four NCs that reflects linear NCs assemblies inside the p-PNC. This assembly is the dominant type for medium and high concentration of NCs (samples C-G). The second configuration CB represents a symmetric cross of five NCs, as shown in **Figure S7a**, and is used to simulate the optical response of more complex 2D and 3D assemblies, as found in samples E-G. As both configurations give very similar results, only the configuration CA is discussed here in detail, while the results obtained for the configuration CB are presented in the supporting information. We calculated absorption

and diffuse reflection cross sections of configuration CA to study both the effects of the NCs spacing distance *a* and that of the electric field polarization. The case of single NC is calculated by using an infinite distance *a* and the corresponding absorption and scattering cross sections are represented by blue dotted lines in **Figures 4b** and **c**, respectively. It is important to note that the calculated dipolar absorption at 475 nm corresponds to the experimentally measured dipolar absorption at 450 nm. The results obtained for the $E_{//}$ polarization, i.e. the electric field oriented parallel to the axis of the linear NCs assembly, are shown in **Figure 4b**. The decrease in *a* spacing from infinity to 2 nm leads to a continuous shift of the inter-cube coupling mode towards longer wavelengths. Additionally, this configuration CA shows a dipolar absorption (marked with red triangle) that is blue-shifted by approximately 15 nm compared to the dipolar absorption band of the single NC. The blue-shift starts to appear for cube spacing of 20 nm and evolves further when cube spacing is reduced to 2 nm, as shown in **Figure 4b**. The mapping of the electric field associated to this band at 462 nm is shown in **Figure 4e** and confirms its dipolar nature thanks to its similarity with the dipolar response of the single NC shown at 475 nm in **Figure 4d**. However, we find also additional electric field intensities between the cubes. In contrast, the mapping of the absorption peak centered at 752 nm corresponds to pure inter-cube coupling, in which the whole plasmonic excitation is only localized between the NCs (**Figure 4f**). The effect of the electric field polarization is presented in **Figure S8a** for NCs spacing of 2 nm. When the electric field is tilted from the $E_{//}$ polarization to the $E_{\perp}$ polarization, i.e. the electric field oriented perpendicularly to the axis of the linear NCs assembly, no inter-cube coupling between the NCs occurs. This is in accordance with studies on polarization dependence on monolayer of silver NCs deposited on dielectric substrates.[7] Furthermore, we observe with this $E_{\perp}$ polarization, likewise for the $E_{//}$ polarization, a blue-shift of the dipolar response which

is even more pronounced in this case. Interestingly, this blue-shift of the dipolar mode under $E_{\perp}$ polarization is already observed with large cube spacing of 20 nm, as shown in **Figure S8c**.

In conclusion, our simulations show that the plasmonic band, which is experimentally observed at 405 nm at the highest NCs density, can be addressed to residual dipolar oscillations of the NCs in combination with weak dipolar coupling, seen under both $E_{//}$ and $E_{\perp}$ polarizations, and strongly enhancing the light absorption in this region. Thus, the almost perfect absorption of the studied p-PNC in the UV is not only related to the high absorption of the high-energy modes in the UV, but also arises from the blue-shift of the strongly absorbing dipolar band due to the formation of NCs assemblies inside the layers.

Reflectance studies

In this section, we present the reflection of the p-PNC more in detail as a function of NCs volume fraction. The total reflectance of the layers deposited on glass was measured by collecting signal in an integration sphere, at near-normal incidence angle of $\theta_{inc} = 8°$. **Figure 5a** shows that the total reflectance spectra, i.e. both specular and diffuse reflections, are strongly modified by NCs density. The minimum in total reflectance is obtained for the highest NCs concentration in sample G, leading to 2.8% and 2.9% at quadrupolar resonance and cubic shape mode wavelengths, respectively. Such a behavior was expected from the high absorption values at these wavelengths. It must be remembered that the p-PNC are deposited on glass and only 5.4% of light signal was transmitted at these wavelengths for this sample G, revealing the high absorption of these nanocomposites. Silver NCs dispersed in PVP at lower density than in the present study were already studied in our previous work.[12] The minima in these reflectance

spectra, which occurred at lower wavelengths than dipolar resonance, were attributed to simultaneous effects of sharp decrease of the refractive index *n* together with sharp increase of the extinction coefficient *k*. The same tendency is seen here in this work for all studied NCs densities. As shown in **Figure 5a**, the reflectance peak of the dipolar resonance at 450 nm increases with the NCs density and gets the strongest reflectance contribution in sample G. This is a consequence of two mechanisms, which is the simultaneous increase in both refractive index and diffuse reflectance despite the high extinction coefficient at this wavelength.

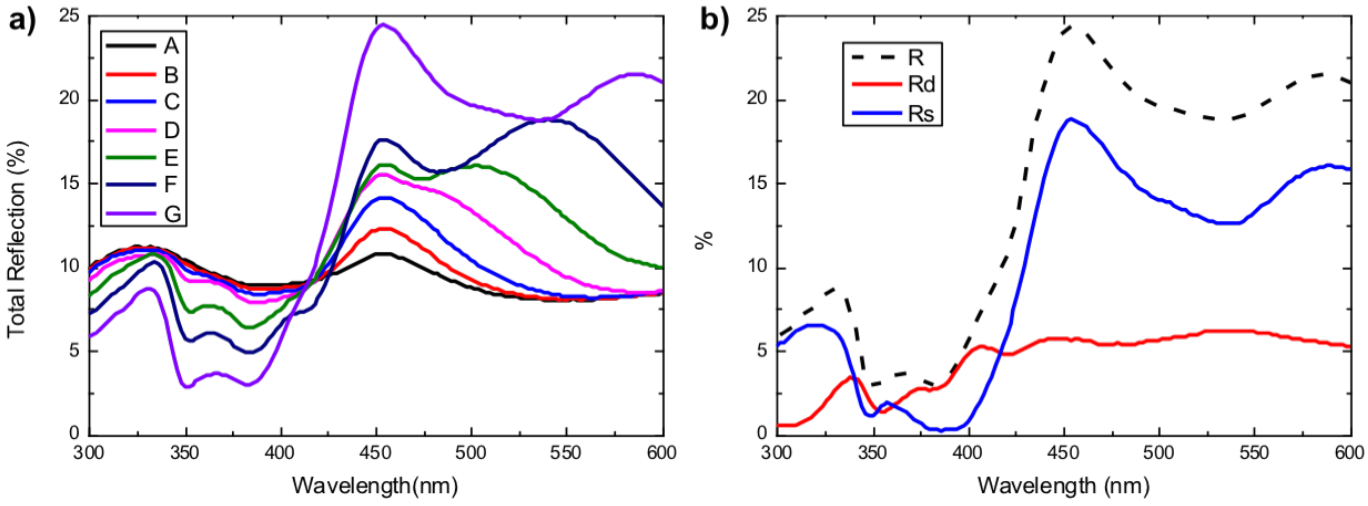

Figure 5. Reflectance spectra of samples A to G (a) and total *R*, diffuse R_d and specular R_s reflectance spectra of sample G (b).

In order to determine the composition of the reflected light, the diffuse reflectance was subtracted from the total reflectance allowing to calculate the specular reflectance. In the case of sample G, the total reflectance at 350 nm of 2.8% is well-balanced between a diffuse reflectance of 1.7% and a specular reflectance of 1.1% (**Figure 5b**). Interestingly, the situation is totally different at the second minima at 384 nm. Here, the total reflectance of 2.9% is mainly due to diffuse reflectance (2.65%) whereas the specular reflectance reaches an extremely low value (0.25%). Considering these encouraging results, we further increase the NCs density to the

highest attainable density, limited by the solubility of the silver NCs, in order to explore the limits of our p-PNC approach towards perfect light absorption. As it can be seen in **Figure S9**, a very low total reflectance of 1.21% is reached at 350 nm that is composed of 0.28% in specular reflectance and 0.93% in residual diffuse reflectance. The results show that the total absorption of our p-PNC can reach values close to 99%. Due to the fact that the silver NCs are highly absorbing in the considered spectral range, we consider that the light trapped inside the p-PNC layer will be re-absorbed by the nanocubes. It has to be pointed out that such high absorption is almost identical to the optical properties of metasurfaces or single-layer gratings used as perfect absorbers,[10,11,47] making our simple solution-processing approach highly interesting for tunable anti-reflecting coatings.

Effects of substrate and angular dependence

This section focuses on the behaviour of specular reflectance on non-transparent substrates in order to avoid residual transmission and to compare the coating performances with more classical systems such as meta-surfaces using sub-monolayers of silver NCs.

The main drawback of metamaterials is that their optical properties are highly dependent on the nature of the underlying substrate, as seen on most of the studies on dielectric,[5] gold or silver substrates.[2,11,48] So far, we demonstrated that nearly zero-reflectance is achievable on glass. **Figure 6a** shows the specular reflectance of the film G spin-coated on various substrates (glass, PET, gold and aluminum). The p-PNC at the NCs density of sample G (8% in volume fraction) shows nearly zero-reflectance (about 0.3%) for all substrates in the region from 380 to 405 nm. The total reflectance, shown in **Figure S10,** is also similar on all substrates in this region as the diffuse reflectance is not influenced by the underlying substrate. Thus, our p-PNC

approach of NCs embedded in PVP has high substrate tolerance to generate zero-reflection in the UV.

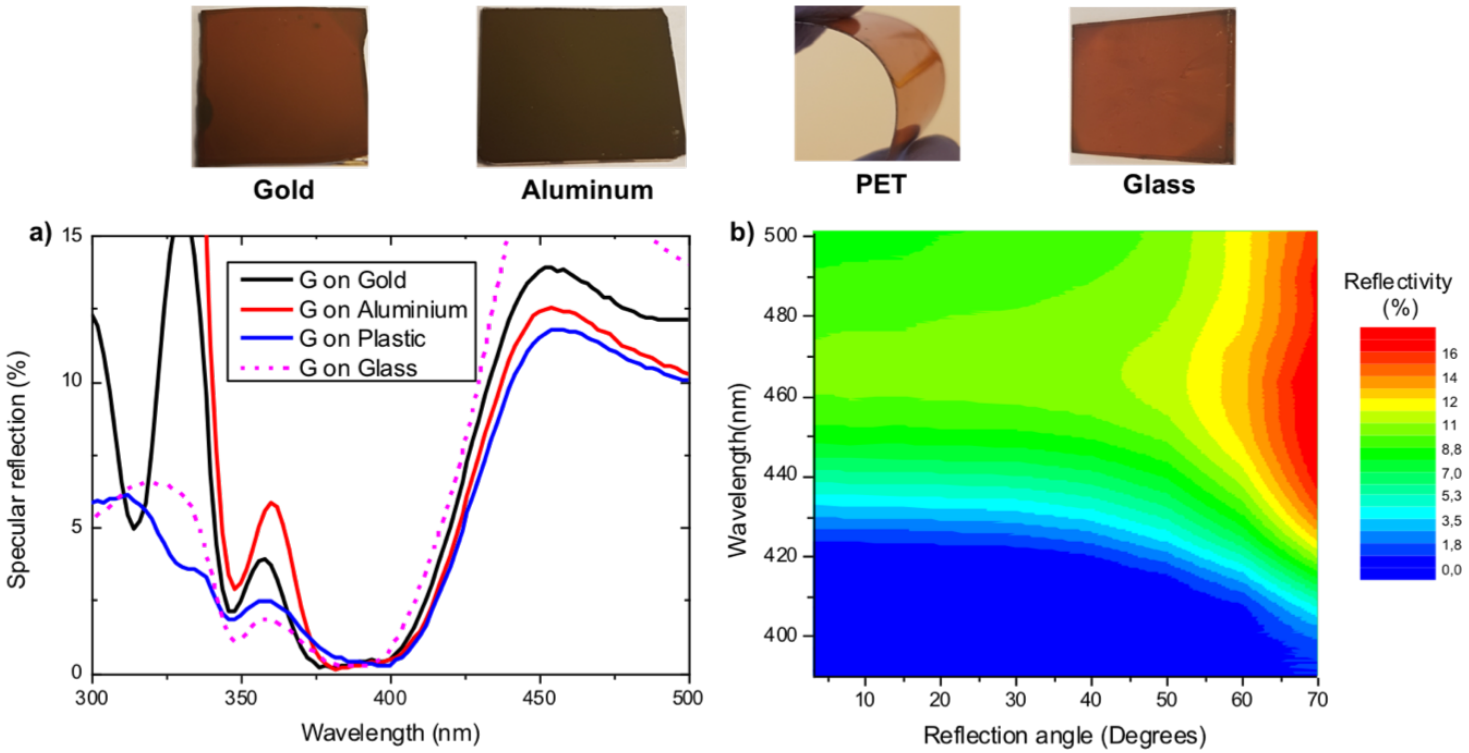

Figure 6. Top part: optical photographs of films using sample G spin-coated on various substrates. Bottom part: Specular reflectance spectra of the resulting films (a) and angular behaviour of the specular reflectance for sample G deposited on aluminum (b).

Furthermore, we studied the angular dependence of the same film G that was deposited on an industrial relevant substrate such as aluminum. It is expected that such layers are less sensitive to the measured angle as compare to other systems, such as meta-surface or ring-resonators systems.[48,49] Angular dependence was measured on the wavelength range from the reflectance minimum to its maximum, i.e. between 390 and 500 nm carried out on a goniometer setup allowing incident angles variations from 3° to 70° (see setup scheme in **Figure S1d**). As it can be seen in **Figure 6b**, the specular reflectance spectrum of film G is nearly constant up to

60°. Importantly, it can be seen in the angular mapping of the specular reflection that the low specular reflection less than 1% between 380 nm to 410 nm exists over a wide-angle region up to the 60° incident angle. This large angular domain of extremely low reflectance shows the advantage of our 3D p-PNC layer approach compared to 2D metasurfaces.[10,50]

Conclusions

We present here plasmonic nanocomposites based on silver NCs embedded in PVP that are produced by a simple one-step solution process on a large palette of substrates of centimeter-sized surface areas. We demonstrate that the optical properties of these nanocomposite films are governed by the density of silver NCs inside the PVP as well as plasmonic couplings between the cubes introduced due to the formation of NCs assemblies with increasing concentration. The absorption of the layers in the visible is governed by inter-cube coupling inside nanocube assemblies leading to additional red-shifted absorption band and limited absorption at the initial wavelength of the dipolar resonance. In contrast, strongly enhanced UV absorption is found at high nanocube densities that is addressed to the absorption of the high-energy modes in the UV in combination with the blue-shifted dipolar band absorption due to the formation of NCs assemblies inside the layers. The enlarged absorption band in the UV shows nearly perfect light absorption of 98.8% that is accompanied by a very weak specular reflection of the layers of only 0.28%. The optical performances in the UV of the presented plasmonic nanocomposite layers, which is demonstrated on different substrates, are comparable to well-known approaches based on 2D assemblies of silver NCs on gold surfaces, making them a promising approach for solution-processed robust and cheap quasi-perfect absorption coatings on a large palette of substrates. Future work will focus on the development of nearly perfect absorption in the visible

spectrum by using metal nanocrystals with plasmonic modes located deeper in the visible spectrum.

ASSOCIATED CONTENT

Supporting Information.

Figures S1 to S10 can be found in the supporting information file.

AUTHOR INFORMATION

Corresponding Authors

* jorg.ackermann@univ-amu.fr ; olivier.margeat@univ-amu.fr

Author Contributions

The manuscript was written through contributions of all authors. All authors have given approval to the final version of the manuscript.

Funding Sources

Work funded by the French “Délégation Générale de l’Armement” (DGA) for the PhD grants of Florent Pourcin and Miriam Carlberg.

ACKNOWLEDGMENT

The authors thank: Serge Nitsche and Damien Chaudanson from CINaM for their assistance in the use of the TEM and SEM facilities; Igor Ozerov and Frédéric Bedu from PLANETE platform at CINaM for substrate preparation; Volkan Kilinc for AFM measurements.

REFERENCES

(1) Faupel, F.; Zaporojtchenko, V.; Strunskus, T.; Elbahri, M. Metal-Polymer Nanocomposites for Functional Applications. *Adv. Eng. Mater.* **2010**, *12* (12), 1177–1190.

(2) Hedayati, M. K.; Faupel, F.; Elbahri, M. Review of Plasmonic Nanocomposite Metamaterial Absorber. *Materials (Basel).* **2014**, *7* (2), 1221–1248.

(3) Hsu, S.-W.; Rodarte, A. L.; Som, M.; Arya, G.; Tao, A. R. Colloidal Plasmonic Nanocomposites: From Fabrication to Optical Function. *Chem. Rev.* **2018**, *118* (6), 3100–3120.

(4) Hore, M. J. A.; Composto, R. J. Nanorod Self-Assembly for Tuning Optical Absorption. *ACS Nano* **2010**, *4* (11), 6941–6949.

(5) Prezgot, D.; Ianoul, A. Probing the Anisotropy of SERS Enhancement with Spatially Separated Plasmonic Modes in Strongly Coupled Silver Nanocubes on a Dielectric Substrate. *J. Phys. Chem. C* **2015**, *119* (6), 3293–3301.

(6) Gao, B.; Arya, G.; Tao, A. R. Self-Orienting Nanocubes for the Assembly of Plasmonic Nanojunctions. *Nat. Nanotechnol.* **2012**, *7* (7), 433–437.

(7) Grillet, N.; Manchon, D.; Bertorelle, F.; Bonnet, C.; Broyer, M.; Cottancin, E.; Lermé, J.; Hillenkamp, M.; Pellarin, M. Plasmon Coupling in Silver Nanocube Dimers: Resonance Splitting Induced by Edge Rounding. *ACS Nano* **2011**, *5* (12), 9450–9462.

(8) König, T. A. F.; Ledin, P. A.; Russell, M.; Geldmeier, J. A.; Mahmoud, M. A.; El-Sayed, M. A.; Tsukruk, V. V. Silver Nanocube Aggregation Gradient Materials in Search for Total Internal Reflection with High Phase Sensitivity. *Nanoscale* **2015**, 5230–5239.

(9) Bottomley, A.; Ianoul, A. Reflection and Absorption Spectra of Silver Nanocubes on a Dielectric Substrate: Anisotropy, Angle, and Polarization Dependencies. *J. Phys. Chem. C* **2014**, *118* (47), 27509–27515.

(10) Akselrod, G. M.; Huang, J.; Hoang, T. B.; Bowen, P. T.; Su, L.; Smith, D. R.; Mikkelsen, M. H. Large-Area Metasurface Perfect Absorbers from Visible to Near-Infrared. *Adv.*

Mater. **2015**, 1–7.

(11) Moreau, A.; Ciracì, C.; Mock, J. J.; Hill, R. T.; Wang, Q.; Wiley, B. J.; Chilkoti, A.; Smith, D. R. Controlled-Reflectance Surfaces with Film-Coupled Colloidal Nanoantennas. *Nature* **2012**, *492* (7427), 86–89.

(12) Carlberg, M.; Pourcin, F.; Margeat, O.; Le Rouzo, J.; Berginc, G.; Sauvage, R.-M. R.-M.; Ackermann, J.; Escoubas, L. Spectroscopic Ellipsometry Study of Silver Nanospheres and Nanocubes in Thin Film Layers. *Opt. Mater. Express* **2017**, *7* (12), 4241.

(13) Teng, C. Y.; Sheng, Y. J.; Tsao, H. K. Surface Segregation and Bulk Aggregation in an Athermal Thin Film of Polymer-Nanoparticle Blends: Strategies of Controlling Phase Behavior. *Langmuir* **2017**, *33* (10), 2639–2645.

(14) Kim, J.; Yang, H.; Green, P. F. Tailoring the Refractive Indices of Thin Film Polymer Metallic Nanoparticle Nanocomposites. *Langmuir* **2012**, *28* (25), 9735–9741.

(15) Li, S.; Meng Lin, M.; Toprak, M. S.; Kim, D. K.; Muhammed, M. Nanocomposites of Polymer and Inorganic Nanoparticles for Optical and Magnetic Applications. *Nano Rev.* **2010**, *1* (1), 5214.

(16) Bottomley, A.; Prezgot, D.; Coyle, J. P.; Ianoul, A. Dynamics of Nanocubes Embedding into Polymer Films Investigated via Spatially Resolved Plasmon Modes. *Nanoscale* **2016**, *8* (21), 11168–11176.

(17) Ahamad, N.; Ianoul, A. Using Phospholipids To Control Interparticle Distance in SERS-Active Substrates. *J. Phys. Chem. C* **2011**, *115* (9), 3587–3594.

(18) Pellarin, M.; Ramade, J.; Rye, J. M.; Bonnet, C.; Broyer, M.; Lebeault, M.-A.; Lermé, J.; Marguet, S.; Navarro, J. R. G.; Cottancin, E. Fano Transparency in Rounded Nanocube Dimers Induced by Gap Plasmon Coupling. *ACS Nano* **2016**, *10* (12), 11266–11279.

(19) Doyle, D.; Charipar, N.; Argyropoulos, C.; Trammell, S. A.; Nita, R.; Naciri, J.; Piqué, A.; Herzog, J. B.; Fontana, J. Tunable Subnanometer Gap Plasmonic Metasurfaces. *ACS Photonics* **2018**, *5* (3), 1012–1018.

(20) Zhang, Q.; Li, W.; Wen, L. P.; Chen, J.; Xia, Y. Facile Synthesis of Ag Nanocubes of 30 to 70 Nm in Edge Length with CF 3COOAg as a Precursor. *Chem. - A Eur. J.* **2010**, *16* (33), 10234–10239.

(21) Michler, G. H. *Electron Microscopy of Polymers*; Springer, 2008.

(22) Rumble, J. R. *CRC Handbook of Chemistry and Physics, 98th Edition, 2017-2018*; 2017.

(23) Xia, Y.; Xiong, Y.; Lim, B.; Skrabalak, S. E. Shape-Controlled Synthesis of Metal Nanocrystals: Simple Chemistry Meets Complex Physics? *Angewandte Chemie - International Edition*. January 2009, pp 60–103.

(24) Tao, A.; Sinsermsuksakul, P.; Yang, P. Polyhedral Silver Nanocrystals with Distinct Scattering Signatures. *Angew. Chemie - Int. Ed.* **2006**, *45* (28), 4597–4601.

(25) Mock, J. J.; Barbic, M.; Smith, D. R.; Schultz, D. A.; Schultz, S. Shape Effects in Plasmon Resonance of Individual Colloidal Silver Nanoparticles. *J. Chem. Phys.* **2002**, *116* (15), 6755–6759.

(26) Lee, H. K.; Lee, Y. H.; Zhang, Q.; Phang, I. Y.; Tan, J. M. R.; Cui, Y.; Ling, X. Y. Superhydrophobic Surface-Enhanced Raman Scattering Platform Fabricated by Assembly of Ag Nanocubes for Trace Molecular Sensing. *ACS Appl. Mater. Interfaces* **2013**, *5* (21), 11409–11418.

(27) Kodiyath, R.; Malak, S. T.; Combs, Z. A.; Koenig, T.; Mahmoud, M. A.; El-Sayed, M. A.; Tsukruk, V. V. Assemblies of Silver Nanocubes for Highly Sensitive SERS Chemical Vapor Detection. *J. Mater. Chem. A* **2013**, *1* (8), 2777.

(28) Liu, X.-L.; Liang, S.; Nan, F.; Yang, Z.-J.; Yu, X.-F.; Zhou, L.; Hao, Z.-H.; Wang, Q.-Q. Solution-Dispersible Au Nanocube Dimers with Greatly Enhanced Two-Photon Luminescence and SERS. *Nanoscale* **2013**, *5* (12), 5368.

(29) Sisco, P. N.; Murphy, C. J. Surface-Coverage Dependence of Surface-Enhanced Raman Scattering from Gold Nanocubes on Self-Asssembled Monolayers of Analyte. *J. Phys. Chem. A* **2009**, *113* (16), 3973–3978.

(30) Sun, Y. Shape-Controlled Synthesis of Gold and Silver Nanoparticles. *Science (80-.).* **2002**, *298* (5601), 2176–2179.

(31) Wang, Y.; Zheng, Y.; Huang, C. Z.; Xia, Y. Synthesis of Ag Nanocubes 18-32 Nm in Edge Length: The Effects of Polyol on Reduction Kinetics, Size Control, and Reproducibility. *J. Am. Chem. Soc.* **2013**, *135* (5), 1941–1951.

(32) Ringe, E.; McMahon, J. M.; Sohn, K.; Cobley, C.; Xia, Y.; Huang, J.; Schatz, G. C.; Marks, L. D.; Van Duyne, R. P. Unraveling the Effects of Size, Composition, and Substrate on the Localized Surface Plasmon Resonance Frequencies of Gold and Silver Nanocubes: A Systematic Single-Particle Approach. *J. Phys. Chem. C* **2010**, *114* (29), 12511–12516.

(33) McMahon, J. M.; Wang, Y.; Sherry, L. J.; Van Duyne, R. P.; Marks, L. D.; Gray, S. K.; Schatz, G. C. Correlating the Structure, Optical Spectra, and Electrodynamics of Single Silver Nanocubes. *J. Phys. Chem. C* **2009**, *113* (7), 2731–2735.

(34) Mahmoud, M. A.; Tabor, C. E.; El-Sayed, M. A. Surface-Enhanced Raman Scattering Enhancement by Aggregated Silver Nanocube Monolayers Assembled by the Langmuir-Blodgett Technique at Different Surface Pressures. *J. Phys. Chem. C* **2009**, *113* (14), 5493–5501.

(35) Lee, S. Y.; Hung, L.; Lang, G. S.; Cornett, J. E.; Mayergoyz, I. D.; Rabin, O. Dispersion in the SERS Enhancement with Silver Nanocube Dimers. *ACS Nano* **2010**, *4* (10), 5763–5772.

(36) Zhou, F.; Li, Z.; Liu, Y. Quantitative Analysis of Dipole and Quadrupole Excitation in the Surface Plasmon Resonance of Metal Nanoparticles. *J. Phys. Chem. C* **2008**, *112*, 20233–20240.

(37) Edwards, P. R.; Sleith, D.; Wark, A. W.; Martin, R. W. Mapping Localized Surface Plasmons within Silver Nanocubes Using Cathodoluminescence Hyperspectral Imaging. *J. Phys. Chem. C* **2011**, *115* (29), 14031–14035.

(38) Zhang, S.; Xu, H. Tunable Dark Plasmons in a Metallic Nanocube Dimer: Toward

Ultimate Sensitivity Nanoplasmonic Sensors. *Nanoscale* **2016**, *8* (28), 13722–13729.

(39) Zacharias, P.; Kliewer, K. L. Dispersion Relation for the 3.8 EV Volume Plasmon of Silver. *Solid State Commun.* **1976**, *18* (1), 23–26.

(40) Nicoletti, O.; de la Peña, F.; Leary, R. K.; Holland, D. J.; Ducati, C.; Midgley, P. A. Three-Dimensional Imaging of Localized Surface Plasmon Resonances of Metal Nanoparticles. *Nature* **2013**, *502* (7469), 80–84.

(41) Ashkarran, A. A.; Daemi, S. Tuning the Plasmon of Metallic Nanostructures: From Silver Nanocubes Toward Gold Nanoboxes. *Plasmonics* **2016**, *11* (4), 1011–1017.

(42) König, T.; Kodiyath, R.; Combs, Z. A.; Mahmoud, M. A.; El-Sayed, M. A.; Tsukruk, V. V. Silver Nanocube Aggregates in Cylindrical Pores for Higher Refractive Index Plasmonic Sensing. *Part. Part. Syst. Charact.* **2014**, *31* (2), 274–283.

(43) Carlberg, M.; Pourcin, F.; Margeat, O.; Le Rouzo, J.; Berginc, G.; Sauvage, R.-M.; Ackermann, J.; Escoubas, L. Optical Response of Heterogeneous Polymer Layers Containing Silver Nanostructures. *Beilstein J. Nanotechnol.* **2017**, *8* (1), 1065–1072.

(44) Kim, S.; Hyun, K.; Struth, B.; Ahn, K. H.; Clasen, C. Structural Development of Nanoparticle Dispersion during Drying in Polymer Nanocomposite Films. *Macromolecules* **2016**, *49* (23), 9068–9079.

(45) Yeshchenko, O. A.; Dmitruk, I. M.; Alexeenko, A. A.; Kotko, A. V; Verdal, J.; Pinchuk, A. O. Size and Temperature Dependence of the Surface Plasmon Resonance in Silver Nanoparticles. *Int. Sch. Conf. Photonics* **2012**, *57* (2), 89.

(46) Ovchinnikov, V. Reflection from Irregular Array of Silver Nanoparticles on Multilayer Substrate. In *ICQNM 2015 : The Ninth International Conference on Quantum, Nano/Bio, and Micro Technologies Reflection*; 2015; pp 16–21.

(47) Xia, S.-X.; Zhai, X.; Huang, Y.; Liu, J.-Q.; Wang, L.-L.; Wen, S.-C. Multi-Band Perfect Plasmonic Absorptions Using Rectangular Graphene Gratings. *Opt. Lett.* **2017**, *42* (15), 3052.

(48) Hedayati, M. K.; Javaherirahim, M.; Mozooni, B.; Abdelaziz, R.; Tavassolizadeh, A.; Chakravadhanula, V. S. K.; Zaporojtchenko, V.; Strunkus, T.; Faupel, F.; Elbahri, M. Design of a Perfect Black Absorber at Visible Frequencies Using Plasmonic Metamaterials. *Adv. Mater.* **2011**, *23* (45), 5410–5414.

(49) Tao, H.; Bingham, C. M.; Strikwerda, A. C.; Pilon, D.; Shrekenhamer, D.; Landy, N. I.; Fan, K.; Zhang, X.; Padilla, W. J.; Averitt, R. D. Highly Flexible Wide Angle of Incidence Terahertz Metamaterial Absorber: Design, Fabrication, and Characterization. *Phys. Rev. B - Condens. Matter Mater. Phys.* **2008**, *78* (24), 2–5.

(50) Huang, F.; Drakeley, S.; Millyard, M. G.; Murphy, A.; White, R.; Spigone, E.; Kivioja, J.; Baumberg, J. J. Zero-Reflectance Metafilms for Optimal Plasmonic Sensing. *Adv. Opt. Mater.* **2016**, *4* (2), 328–335.

FOR TABLE OF CONTENTS USE ONLY

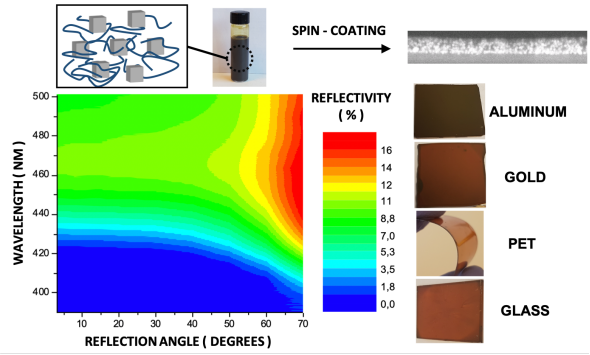

Silver nanocubes-embedded polymer thin films display UV absorption as high as 98.8% and specular reflection of only 0.28% independently on the underlying substrates.